Materials Research. 2023; 26(suppl. 1): e20220572
DOI: https://doi.org/10.1590/1980-5373-MR-2022-0572

Assessment of the Von Mises Stresses and Stress Triaxiality in Notches Using Modified Tensile Specimens

***Letícia dos Santos Pereira*[a]*, *Gustavo Henrique Bolognesi Donato*[b], *Miguel Mattar Neto*[a]**

[a]*Instituto de Pesquisas Energéticas Nucleares (IPEN), 05508-000, São Paulo, SP, Brasil.*
[b]*Centro Universitário FEI, 09850-901, São Bernardo do Campo, SP, Brasil.*

Received: December 15, 2022; Revised: April 10, 2023; Accepted: May 03, 2023

Complete understanding of the local stress triaxiality and stress concentration is essential to ensuring structural safety of several structures. A combination of mechanical tests with numerical simulations can be used to obtain this information. One way to study stress triaxiality is by modifying the standard tensile test geometry (ASTM E8) with a notch. Based on previous results from the literature, five notches were chosen: 10, 5, 3, 2, and 1 mm. These geometries were tested, and the results were numerically reproduced using the Abaqus/Explicit 2020 software. The models used were a non-linear model with the Gurson-Tvergaard-Needleman damage model to reproduce the failure. The numerical analyses allowed the assessment of the von Mises stress and stress triaxiality near the notch to compare with the standard smooth specimen. Two instants were considered as crack propagation onset; the instant of the maximum von Mises stress in the element at the center of the specimen, where the failure process begins; and the moment of maximum stress in the true stress x true strain curve. For the von Mises stress analysis, the difference between the curves was small. The stress triaxiality is a better variable to visualize the influences of the notch. When the strain is equal to a 0.07 (instant of the maximum force for the standard specimens), for the smaller notches (1 and 2 mm), there is a region where the effective plastic strain is zero. Consequently, the stress triaxiality is larger in this region than in the center. For the crack propagation onset instant, the plastic strain occurs along the whole transversal section. In this instant, the maximum value of stress triaxiality occurs in the center for all specimens. These results demonstrate that the stress triaxiality changes as the strain increases, i.e., varies with time.

Keywords: *Tensile test, stress triaxiality, von Mises stress, GTN model, notch.*

1. Introduction

Stress triaxiality is important in fracture mechanics to check the safety of several structures, e.g., pipelines, nuclear reactors, airplanes, etc. The formula used to define the stress triaxiality is the ratio of hydrostatic (mean) stress (σ_m) to von Mises (equivalent) stress (σ_e), i.e., σ_m/σ_e [1]. Stress triaxiality is one of the main factors that influence the fracture process of high-toughness steels. For example, a ductile fracture tends to be more prevalent for a low-constraint geometry with less plastic restriction. This means that if the constraint is low the restriction for plastic deformation is small, therefore favoring a ductile fracture. The configuration and loading of the structural components are different from those of the mechanical test specimens used to obtain the material fracture properties[1,2]. Therefore, understanding local stress triaxiality is fundamental to ensure structural safety.

Understanding the stress distribution near the fracture region is also essential to the fracture process. Numerical and experimental results permit more important information and field descriptions. The simulations must be non-linear with a damage model to reproduce failures. The stress triaxiality could affect the calibration of the parameters of some damage models, including the Gurson-Tvergaard-Needleman model (GTN). Depending on the stress triaxiality, the calibrated parameters might be different for the same material. However, each model has its particularities.

GTN is a well-known model based on the ductile fracture process. The model considers the nucleation of microvoids, the growth, and the coalescence of the voids resulting in the failure[3-6]. This is an advantage compared with other models. However, nine parameters are necessary to model the failure process. In Abaqus (2020), the parameters are q_1, q_2, q_3, f_c, f_F, f_N, σ_N, ε_N, and r_0 [7]. The first three (q_1, q_2, q_3) are constitutive parameters and are independent of the material; q_1 responds by a decrease in the force because of the interaction of the voids; q_2 and q_3 control the stress triaxiality and volume fraction void effect, respectively[8,9]; the parameters f_N, σ_N, and ε_N are the secondary nucleation parameters;. ε_N is the plastic strain at the nucleation of new voids, and as this nucleation follows a normal distribution ε_N is the mean value; and σ_N is the standard deviation. In addition, f_N is the volume of void nucleation particles[5]. The other material parameter, r_0, is the initial relative density, i.e., the initial ratio of the volume of solid material to the total volume of the material[7,9]. Lastly, f_c and f_F are the parameters of the failure criteria, the first one is the critical parameter, and the second is the void volume fraction at which the element is removed. If the volume

*e-mail: lspereira391@gmail.com

fraction is between f_c and f_F, the micro-fracture mechanisms and void coalescence occur[7]. To facilitate the calibration, q_1, q_2 and q_3 can be considered equal to 1.5, 1.0, and 2.25, repectively[7,9-13]. Furthermore, some authors[10-13] recommend, for steel, $\varepsilon_N = 0.3$, $\sigma_N = 0.1$, and $f_c = 0.02$. Lastly, r_0 varies between 0.0001 and 0.0003[10-13].

One method to evaluate stress triaxiality is by modifying a standard tensile test geometry with an external circumferential notch. The standard specimen is a cylindrical bar (smooth round bar) based on the ASTM E8/E8M standard[14]. Several studies were carried out with different diameters and notch radii[12,15-20]. As the minimum diameter varies for each study, it is interesting to use the ratio of the radius (R) and minimum diameter (ϕ_{min}). Derpenski and Seweryn[15] tested 24 combinations of R/ϕ_{min}, ranging from 0.038 to 5. Moreover, the values of R/ϕ_{min} found in the literature are 0.167, 0.2, 0.24, 0.25, 0.312, 0.333, 0.5, 0.667 0.78, 1.0, 1.5[12,16-20].

Studies show that it is possible to obtain the critical plastic fracture strain $\varepsilon_{p,crit}$ relative to stress triaxiality, Equation 1[18,20-24]. The parameters α and β, Equation 1, are constants of the material and can be calibrated using results of tensile tests with different notches[20]. Some authors consider a β constant equal to 1.5[22-24]. However, the best option is to calibrate them using the values of $\varepsilon_{p,crit}$, σ_m, and σ_e obtained for the instant of crack propagation onset. Both Bao[18] and Ruggieri[20] consider the instant before the stress decreases, of the true stress (σ) vs. true strain (ε) curve. Bao[18] used the element located in the center of the specimen. Alternatively, Ruggieri[20] considered the elements with porosity $f = 0.1$, analyzing JIS STPT370 steel, a material also applied to pipelines. Using the same material, Plata Uribe et al.[21] applied a different methodology to discover α and β. The point of the crack propagation onset was obtained experimentally and used as the correspondent point in the simulation. These are the values used in the SMCS (Stress-Modified Critical Strain) damage model[21,24].

$$\varepsilon_{p,\,crit} = \alpha \exp\left(-\beta \frac{\sigma_m}{\sigma_e}\right) \tag{1}$$

2. Methodology

The material used is a steel API X65 sour, classified by the API 5L standard[25]. This material is applied in pipelines of the oil and gas industry because of its high toughness. The number after the letter X is the yield stress in ksi[25]. The specimens were machined from sheets cut from a gas pipeline. The thickness of the sheets is 20.69" (0.53 m).

Two standard[14] specimens were tested, one with a minimum diameter of 12.3 mm (S12), Figure 1(a), and the other with a diameter of 10 mm (S10), Figure 1(b). Five notched specimens were also tested. The notches were machined from specimen S12 with a minimum diameter of 10 mm, only varying R, Figure 1(c). The radii of the notches are 10 mm (N10), 5 mm (N5), 3 mm (N3), 2 mm (N2), and 1 mm (N1), and, consequently, the R/ϕ_{min} values are 1.0, 0.5, 0.3, 0.2, and 0.1, respectively.

Tests were performed on an MTS machine with a test speed of 0.9 mm/min (0.015 mm/s). For greater precision, an extensometer was used to obtain the strain. Additionally, two cameras, Figure 2, were used to obtain the minimum diameter and the radii after yielding for several instants. The cameras enable the true stress vs. true strain curve until total fracture to be obtained. Because of the anisotropy, the deformation is not constant in the cross-section, so two cameras provide the information to calculate the elliptical resistant area. The only part of the anisotropy that was considered in this study was the elliptical area. The anisotropy model is not available in Abaqus (2020) when the GTN model is used.

The FEA code used in this study is Abaqus (2020). The geometries were simulated in the Abaqus/Explicit, using a non-linear model. The non-linear effects are caused by the larger displacement and the elasto-plastic material properties. Using a non-linear model is fundamental for reproducing the test, because of the large plastic deformation that the specimen suffers before failure. The properties of the material were obtained from the test of the two specimens, following the ASTM E8 standard[14] (S12 and S10). For this, the procedure described in the standard[14] was followed, and the modulus of elasticity (E) and stress vs. strain curves were

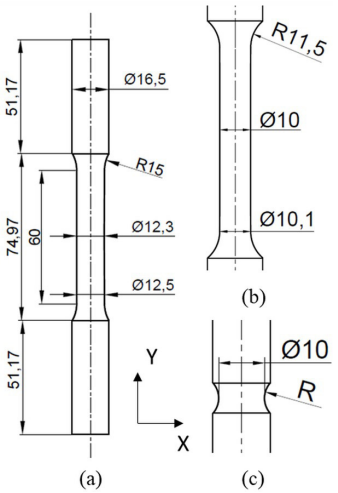

Figure 1. Geometries: (a) S12; (b) S10; and (c) notched specimen.

Figure 2. Setup of the tensile test machine.

obtained for the test. Using the real area, the real stress vs. stain curves were obtained, and these curves were corrected by the Bridgman[26] method. Then a routine in Matlab was developed to obtain the average curve and modulus of elasticity. The elastic properties are E = 205.05 GPa and Poisson (ν) = 0.33. The ν utilized is a well-known value found in the literature. Thus, the plastic property inputs were points of the true stress vs. true strain curve, as shown in Figure 3. As the simulation is dynamic, so the density must be informed. The steel density is on average 7.85 g/cm^3. The units used in the simulation are mm for length, Newton for strength, second for time, and MPa for stress. Because of this, the density needs to be in ton/mm^3. Therefore, the density is 7.85×10^{-9} ton/mm^3.

The model is axisymmetric with symmetry in the longitudinal direction (Y-symmetry). Because of the GTN the model must be explicit dynamic, allowing larger displacements, which means a large strain theory is being applied. The mesh is refined in the Y-symmetry region, where the damage propagates. Additionally, the smallest element has dimensions of 0.2 x 0.1 mm, near the Y-symmetry, and the largest is 1.0 x 1.0 mm in the diameter 16.5 mm. The total elements are shown in Table 1. The elements are Quad (four nodes) with reduced integration, i.e., the calculations are performed for the center of the element. This reduced integration is needed when the GTN is used. The displacement in the Y direction of the Y-symmetry nodes was fixed (0). First, a test speed of 0.015 mm/s was applied in the Y direction, but convergence problems occurred. The time increment to achieve convergence in these simulations, needs to be very small. The problem is the density is very low, 7.85×10^{-9}, as explained above. When the speed is low, the step time is larger, and consequently many increments are necessary. Using a test speed of 0.015 mm/s, more than 20,000,000 increments are necessary, causing errors. By increasing the speed, the step time is smaller, and therefore fewer increments are necessary, solving the problem. Thus, the speed was increased to 100 mm/s. In this case, the strain rate effect is not modeled. Some tests were performed with speeds of 10, 25, 50, 75, and 100 mm/s. The true stress x true strain curves obtained coincide, independent of the speed used. Thus, the results of the stress triaxiality and von Mises stress were also the same. Using 100 mm/s, the step time for each geometry is shown in Table 1.

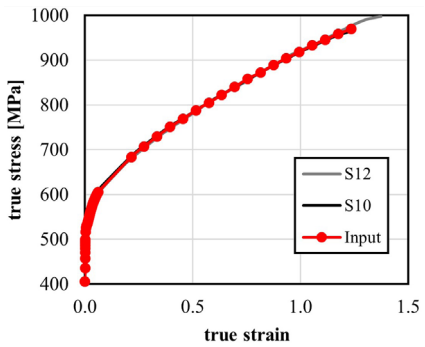

Figure 3. Input of plastic properties.

The GTN model has nine parameters to calibrate. Therefore, to facilitate this calibration, all the parameters, except f_N, were fixed, based on the literature information[5,9-13]. Then the calibration was performed, changing the f_N value until reproduction of the experimental curve. The only parameters that are independent of the materials are q_1, q_2 and $q3$. However, normally these parameters are considered fixed by several authors and equal to 1.5, 1.0, and 2.25, respectively. Before the calibration, a statistical analysis was performed and the f_N was the most statistically relevant parameter. Thus, using the f_N to calibrate the curve is interesting. In the literature instead of $r_{0.}$ the parameter $f_{0.}$ the initial volume fraction of voids, is used. So, $r_0 = 1 - f_{0.}$ In the test performed prior to the calibration this was the parameter that least affected the result. Therefore, the chosen value for r_0 is 0.9997. The critical parameter chosen for f_c, from which the damage process is accelerated, was 0.03. The fraction of void volume in the fracture, f_F, is calculated using Equation 2, in relation to q_1, q_2, q_3, f_c, and the damage acceleration factor κ[10]. Consequently, $f_F = 0.1892$. The values chosen for the two secondary nucleation parameters besides f_N are ε_N = 0.3 and σ_N = 0.1. Table 2 shows the calibrated f_N values for each geometry. The differences between the values are considerable. This is noteworthy because the material is the same, i.e., the same constitutive model. The only difference between the specimens is the triaxiality. This proves that the values of the parameters are different depending on the triaxiality. In this study, the calibration was performed by varying the f_N, but the calibration could be carried out by changing the values of the other parameters. As the q_2 controls the stress triaxiality it should not be constant and equal to 1.0 and should be calibrated for each geometry.

Table 1. Elements and step time used in the simulations.

Specimen	Elements	Step Time
S10	2152	0.054
S12	2586	0.065
N10	2758	0.030
N5	2537	0.030
N3	2472	0.030
N2	2617	0.030
N1	2479	0.026

Table 2. Calibration of the f_N parameter of GTN.

Specimen	f_N
S10	0.00015
S12	0.00045
N10	0.00060
N5	0.00050
N3	0.00045
N2	0.00100
N1	0.00170

$$f_F = \frac{\frac{q_1 + \sqrt{q_1^2 - q_3}}{q_3} - f_c}{\kappa} + f_c \quad (2)$$

Using a Python routine, the values of stress, stress triaxiality, and effective plastic strain were obtained for the centroid of the elements, and the coordinate values for the nodes. The values were obtained for the centroid because the reduced integration was used, and therefore the value is not available for the nodes. The organization of values and the calculations were performed using a Matlab routine that wrote the results in Excel.

Three instants in time were chosen to perform the analyses. The first (instant 1) is the moment of maximum force of the standard specimen. The displacement measured by the virtual extensometer for the S10 was used to determine the instant for the notched specimen. Considering that the virtual extensometer is a set of nodes created in the position corresponding to the place where the extensometer was positioned during the test, instant 1 was considered when the displacement was equal to the S10. The second, instant 2, is the moment of the maximum von Mises stress in the central element (the element close to the axisymmetric axis and the Y-symmetry line), Figure 4(a). The central element is the first one to start to fail. Then, instant 3 is the moment of maximum stress in the true stress x true strain curve.

The effective plastic strain (PEEQ) related to the stress triaxiality (T) curve[18,20] must be obtained at the crack propagation onset. The problem is to determine the instant at which the crack is about to start propagating. Normally, the point of maximum stress on the true stress x true strain curve is considered (instant 3)[18,20,21]. However, the stress in the elements starts to decrease before this instant. Thus, instant 2 was also considered.

In addition, two elements were considered: the central element, Figure 4(a), and the element with the volume void on the crack propagation onset, $f = 0$.

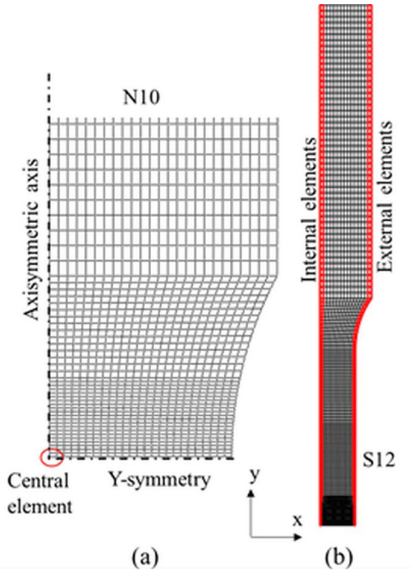

Figure 4. (a) central element and symmetries; (b) internal and external elements.

The analysis of the von Mises stress (SvM) variation on the Y coordinates was carried out at two instants in time, 1 and 2. Instant 3 was not considered because the von Mises stress started to decrease because of the damage. Two sets of elements were used: the axisymmetric (internal) and the free surface (external). These sets are shown in Figure 4(b).

Finally, the stress triaxiality in relation to the relative radius was studied. The analyzed elements were those in Y-symmetry. The relative radius was calculated by dividing the distance between the element centroid and the axisymmetric axis (r) by the maximum radius(r_{max}). The analysis was also performed for instants 1 and 2.

3. Results and Discussion

Figure 5 shows the PEEQ vs. T curves. For Figure 5(a), the values were obtained for the central element, Figure 4, at instant 3. The points do not follow a clear trend. So, after that, the values were obtained in the same element, but for instant 2, Figure 5(b). In this case, it was possible to use an exponential fit with a high R^2. The parameters α and β are obtained from the regression analysis made in Excel to plot the exponential fit, shown in the equations in Figure 5(b) and Figure 5(c). Considering Equation 1, α is the constant and β is the exponent that multiplies the stress triaxiality. Finally, the third analysis was based on the study of Ruggieri[20]. The values were obtained for the element with a void volume, f, equal to 0.1 at instant 3. This methodology also allowed the regression analysis, with an R^2 slightly smaller than the one in Figure 5(b). The values of α and β found by Ruggieri[20] are 1.77 and 0.5, respectively, close to the values obtained in Figure 5(c). On the other hand, Plata Uribe et al.[21] found $\alpha = 4.2$ and $\beta = 1.7$, which are closer to the values shown in Figure 5(b). Considering only the notched specimen, the values change. For Figure 5(b), the values changed from $\alpha = 6.3$ and $\beta = 1.9$ to $\alpha = 5.6$ and $\beta = 1.8$, while, for Figure 5(c) they changed from $\alpha = 2.6$ and $\beta = 0.9$ to $\alpha = 2.0$ and $\beta = 0.7$. These results are closer to Ruggieri[20] and Plata Uribe et al.[21] than to the standard specimens. As all the results have the same order of magnitude, this indicates that the numeric models present good agreement with the predicted results. Better understanding of the crack propagation onset instant is recommended to use the SMCS damage model. The main point is the moment when the damage started. For example, instant 3, is immediately prior to the deletion of the first element. However, as shown before, the element degradation has been going on for some time. The methodology presented by Ruggieri[20] does not use the central element, because this element is already failing. Finally, the SMCS was not used in this study since we used the GTN model. The SMCS is simpler than GTN, but it is not available in Abaqus (2020).

The analysis of the numerical results enabled the assessment of the variation in the von Mises stress concerning coordinates in the Y direction. Figure 6(a) shows this variation for instant 1 for all specimen lengths and detailed for gauge length. The first observation is related to the notch influence until approximately 30 mm (gauge length). As shown in Figure 1, this is the limit of the minimum parallel length. For the standard specimen, the stress is practically constant in this region. Alternatively, for the notched specimens, the von Mises stress is concentrated at the Y-symmetry, followed

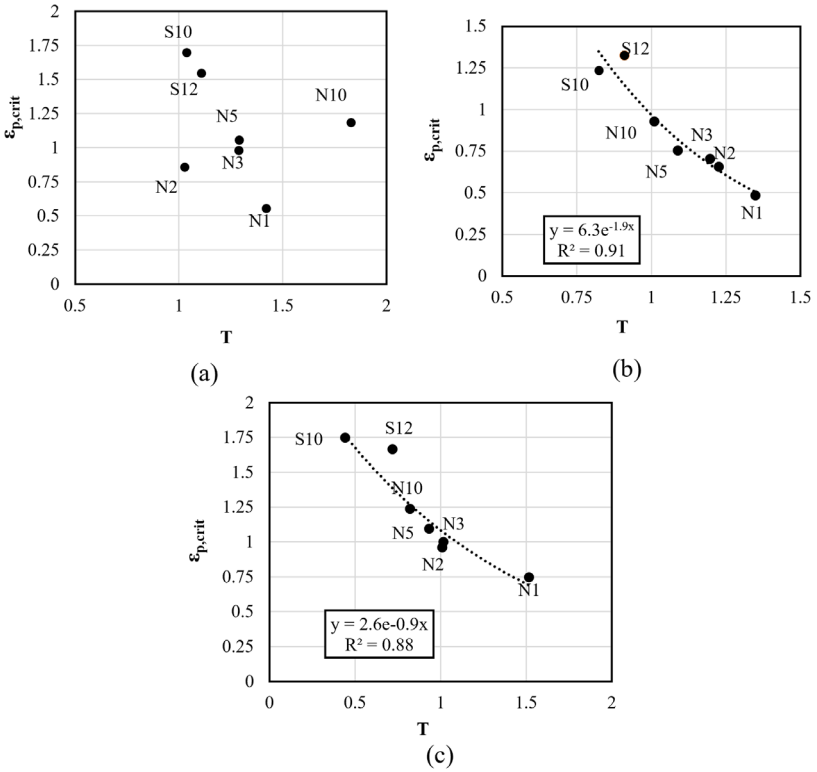

Figure 5. effective plastic strain vs. triaxiality: (a) central element for instant 3, (b) central element for instant 2, (c) element with $f = 0.1$ for instant 3.

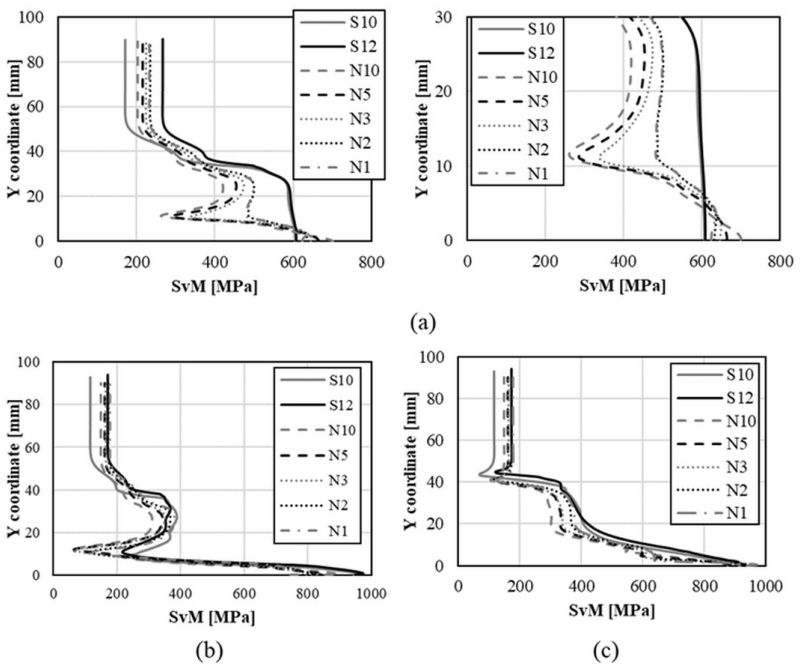

Figure 6. Y coordinate vs. von Mises stress: (a) internal elements for instant 1, (b) internal elements for instant 2, (c) external elements for instant 2.

by a decrease in stress. For the smaller radii (N2 and N1), the decrease is smaller; the stress is more concentrated in the notch. The same occurs for instant 1, Figure 6(b). For instant 2, the standard specimen behavior is the same for the notched specimens. For the external elements, Figure 6(c), between approximately 15 and 40 mm, the von Mises stress for the standard specimens is larger than for the notched specimens, mainly for the N10, N5, and N3. The deformation causes

the increasing radius of the notch. On the other hand, for the standard specimens, after plastic instability (necking), the radius decreases. Therefore, the stress becomes closer to the smaller radius. Before the maximum force, it is possible to visualize the influence of the notch for the standard specimens. After that, because of the necking, the difference is not significant. Consequently, the von Mises stress is not the best variable to identify the length of the region affected by the notch after necking.

Figure 7 shows the stress triaxiality in the minimum diameter (Y-symmetry). For instant 1, Figure 7(a), the stress triaxiality for the S10 and S12 coincide. Furthermore, the stress state is practically uniaxial. For the N10 and N5, the largest stress triaxiality is in the center of the specimen. For the N3, the stress triaxiality close to the center is constant. Then, for N2 and N1, the curve is utterly different; the large stress triaxiality is close to the notch. The plastic strain in the notch region causes an area where the effective plastic strain is close to zero, as shown in Figure 8(a). The constraint in this region increases relative to the specimen center. On the other hand, for the N10, N5, and N3 specimens, the effective plastic strain in all Y-symmetry is different from zero, as shown for the N10, in Figure 8(b). For instant 2, Figure 7(b), all the curves follow the same trend. The plastic strain occurs in all the Y-symmetry for all specimens. For the standard specimens, the necking causes the same effect as the notch; however, in this study, the difference between the curves is more significant. Furthermore, the stress triaxiality changes as the strain increases, so the region where the notch affects the results changes with time. Consequently, the more instants analyzed the better.

The last analysis was the stress triaxiality (T) vs. the plastic stain (ε_p), shown in Figure 9. For the standard smooth specimen, S10 and S12, after the plastic instability (necking) the stress triaxiality starts to increase. Initially this increase is modest, then, after a plastic strain equal to 0.2 this increase becomes substantial. For the notched specimens N10, N5, and N3, the smaller the radius notch the greater the stress triaxiality. The stress triaxiality at the start of the curve for N2 and N1 is smaller than expected. Nevertheless, the variation in the stress triaxiality in relation to the plastic strain is larger than for the other specimens.

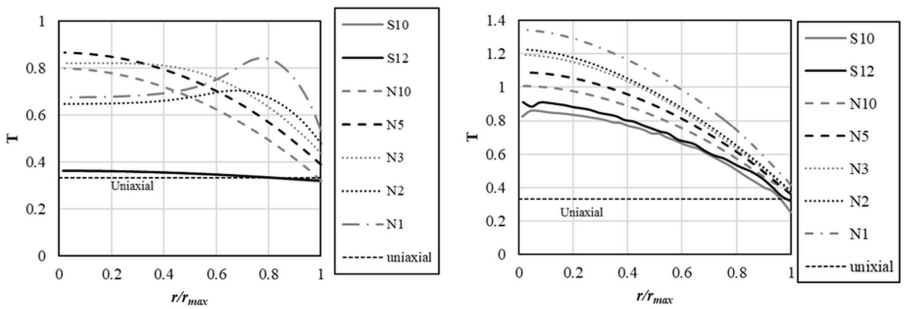

Figure 7. Triaxiality vs. relative radius: (a) instant 1, (b) instant 2.

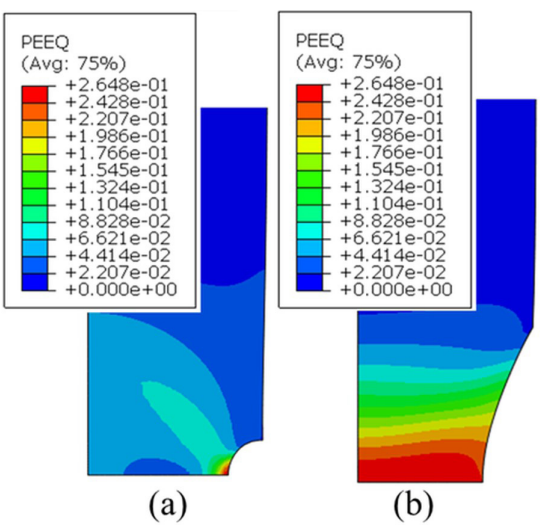

Figure 8. Effective plastic strain at instant 1 for the: (a) N1, (b) N10.

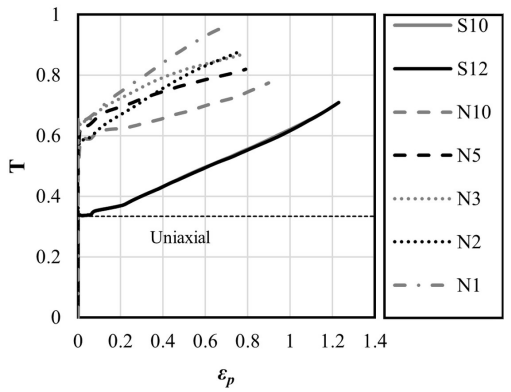

Figure 9. Stress triaxiality vs. von Mises stress.

4. Conclusion

The calibration of the f_N was chosen because it is the most statistically relevant parameter. The values are different for each geometry, proving the influence of the stress triaxiality on the GTN parameters. However, the calibration could be performed for any parameter. The next step would be to calibrate the q_2, maintaining f_N constant, then to obtain the graphics and compare with these results.

Based on the literature, it was possible to obtain an exponential curve relating the critical plastic fracture strain to the stress triaxiality. The main difficulty was to determine the crack propagation onset instant. Two methodologies were proven to be adequate. The values of α and β obtained had the same order of magnitude as values found in the literature, indicating that the numeric models agree with the predicted results. However, better understanding of when the failure begins is recommended.

The numerical results allowed the study of the stresses in different points of the specimen. Before the ultimate tensile strength for the standard specimens, it is possible to observe the effect of the notch on von Mises stress. However, at crack propagation onset, the difference between the curves is small, and therefore, the von Mises stress is not the best variable to identify the length of the region affected by the notch after the necking.

The largest value of stress triaxiality is close to the notch for the smaller radius (N2 and N1) and instant 1. A large plastic strain in the notch causes a region where the plastic strain is close to zero for this instant. Therefore, the stress triaxiality in this region is larger. After the plastic strain occurs in all Y-symmetry, the maximum value of stress triaxiality occurs in the center. For instant 2, the curves followed the same trend. The plastic strain occurs in all the Y-symmetry for all specimens. For the S10 and S12, the neck causes the same effect as the notch. The stress triaxiality is a better variable to visualize the influence of the notch on stress states and plasticity evolution.

For the S10 and S12 after the plastic instability, the stress triaxiality starts to increase. Initially, this increase is modest, then, after a plastic strain equal to 0.2 this increase becomes substantial. For the N10, N5, and N3, the smaller the radius notch the greater the stress triaxiality. For the N2 and N1, the variation in stress triaxiality is larger than for the other specimens.

It is concluded that the numerical results enable the visualization of the effect of the notch mostly in the minimum diameter (Y-symmetry) using the stress triaxiality. Finally, the stress triaxiality changes as the strain increases, so the region where the notch affects the results varies with time. For future considerations, more instants should be analyzed to better understand how stress triaxiality changes with time.

5. Acknowledgments

The present research was supported by the Instituto de Pesquisas Energéticas Nucleares (IPEN), Conselho Nacional de Desenvolvimento Científico e Tecnológico (CNPq), and Centro Universitário FEI.

6. References

1. Darlet A, Desmorat R. Stress triaxiality and Lode angle along surfaces of elastoplastic structures. Int J Solids Struct. 2015;67–68:71-83. http://dx.doi.org/10.1016/j.ijsolstr.2015.03.006.
2. Anderson TL. Fracture mechanics: fundamentals and applications. 4th ed. Boca Raton: CRC Press; 2017.
3. Gurson AL. Continuum theory of ductile rupture by void nucleation and growth: Part I—yield criteria and flow rules for porous ductile media. J Eng Mater Technol. 1977;99:2-15. http://dx.doi.org/10.1115/1.3443401.
4. Tvergaard V, Needleman A. Analysis of the cup-cone fracture in a round tensile bar. Acta Metall. 1984;32:157-69. http://dx.doi.org/10.1016/0001-6160(84)90213-X.
5. Ruggieri C, Panontin TL, Dodds RH. Numerical modeling of ductile crack growth in 3-D using computational cell elements. Int J Fract. 1996;82:67-95. http://dx.doi.org/10.1007/BF00017864.
6. Tvergaard V. Material failure by void growth to coalescence. In: J. Hutchinson, T. Wu, editors. Advances in applied mechanics. New York: Academic Press; 1989. p. 83-151.
7. Simulia. Abaqus documentation. Rode Island: Simulia; 2020.
8. Zhang ZL. A sensitivity analysis of material parameters for the Gurson constitutive model. Fatigue Fract Eng Mater Struct. 1996;19:561-70. http://dx.doi.org/10.1111/j.1460-2695.1996.tb00992.x.
9. Kiran R, Khandelwal K. Gurson model parameters for ductile fracture simulation in ASTM A992 steels. Fatigue Fract Eng Mater Struct. 2014;37:171-83. http://dx.doi.org/10.1111/ffe.12097.
10. Nonn A, Kalwa C. Analysis of dynamic ductile fracture propagation in pipeline steels: a damage-mechanics' approach. In: 6th International Pipeline Technology Conference, Tiratsoo Technical; Ostend, Belgium. Proceedings. Beaconsfield: Tiratsoo Technical; 2013. p. 1419-38. https://doi.org/10.13140/2.1.4370.3046.
11. Scheider I, Nonn A, Völling A, Mondry A, Kalwa C. A damage mechanics based evaluation of dynamic fracture resistance in gas pipelines, Procedia. Mater Sci. 2014;3:1956-64. http://dx.doi.org/10.1016/j.mspro.2014.06.315.
12. Li W, Liao F, Zhou T, Askes H. Ductile fracture of Q460 steel: effects of stress triaxiality and Lode angle. J Construct Steel Res. 2016;123:1-17. http://dx.doi.org/10.1016/j.jcsr.2016.04.018.
13. Moço RF. Correlação da fenomenologia da fratura dúctil de gasodutos e corpos de prova dinâmicos Charpy e DWTT empregando o modelo GTN a aços avançados classe API [dissertation]. São Paulo: Centro Universitário FEI; 2017.
14. ASTM: American Society for Testing and Materials. ASTM E8/E8M: standard test methods for tension testing of metallic materials. West Conshohocken: ASTM; 2020. https://doi.org/10.1520/E0008_E0008M-16AE01.
15. Derpenski L, Seweryn A. Numerical analysis of the strain and stress state in cylindrical in notched tensile specimens. Mater Sci. 2013;49:252-6.

16. Keshavarz A, Ghajar R, Mirone G. A new experimental failure model based on triaxiality factor and Lode angle for X-100 pipeline steel. Int J Mech Sci. 2014;80:175-82. http://dx.doi.org/10.1016/j.ijmecsci.2014.01.007.
17. Algarni M, Bai Y, Choi Y. A study of Inconel 718 dependency on stress triaxiality and Lode angle in plastic deformation and ductile fracture. Eng Fract Mech. 2015;147:140-57. http://dx.doi.org/10.1016/j.engfracmech.2015.08.007.
18. Bao Y. Dependence of ductile crack formation in tensile tests on stress triaxiality, stress and strain ratios. Eng Fract Mech. 2005;72:505-22. http://dx.doi.org/10.1016/j.engfracmech.2004.04.012.
19. Kondori B, Benzerga AA. Effect of stress triaxiality on the flow and fracture of Mg alloy AZ31. Metall Mater Trans, A Phys Metall Mater Sci. 2014;45:3292-307. http://dx.doi.org/10.1007/s11661-014-2211-7.
20. Ruggieri C. Numerical investigation of constraint effects on ductile fracture in tensile specimens. J Braz Soc Mech Sci Eng. 2004;26:190-9.
21. Plata Uribe YA, Ruggieri C, Ohata M. A strain-based criterion to assess ductile failure initiation in dented pipelines under tensile loading. J Strain Anal Eng Des. 2021;56:359-70. http://dx.doi.org/10.1177/0309324720975273.
22. Marini B, Mudry F, Pineau A. Experimental study of cavity growth in ductile rupture. Eng Fract Mech. 1985;22:989-98.
23. Huang Y, Hutchinson W, Tvergaard V. Cavitation instabilities in elastic-plastic solids. J Mech Phys Solids. 1991;39:223-41. http://dx.doi.org/10.1016/0022-5096(91)90004-8.
24. Smith C, Kanvinde A, Deierlein G. A local criterion for ductile fracture under low-triaxiality axisymmetric stress states. Eng Fract Mech. 2017;169:321-35.
25. API: American Petroleum Institute. API 5L: specification for line pipe. Washington, DC: API; 2013.
26. Bridgman PW. Studies in large plastic flow and fracture. 1st ed. New York: Mcgraw-hill Book Company; 1952. The effect of nonuniformities of stress at the neck of a tension specimen, p. 9-37.